Spectral crossover in non-hermitian spin chain systems : comparison with random matrix theory

Ayana Sarkar,* Sunidhi Sen,† and Santosh Kumar[‡] Department of Physics, Shiv Nadar Institution of Eminence, Gautam Buddha Nagar, Uttar Pradesh-201314, India

(Dated: February 6, 2023)

We systematically study the short range spectral fluctuation properties of three non-hermitian spin chain hamiltonians using complex spacing ratios. In particular we focus on the non-hermitian version of the standard one-dimensional anisotropic XY model having intrinsic rotation-time-reversal symmetry that has been explored analytically by Zhang and Song in [Phys.Rev.A 87, 012114 (2013)]. The corresponding hermitian counterpart is also exactly solvable and has been widely employed as a toy model in several condensed matter physics problems. We show that the presence of a random field along the x-direction together with the one along z facilitates integrability breaking and emergence of quantum chaotic behaviour indicated by a spectral crossover resembling Poissonian to Ginibre unitary (GinUE) statistics of random matrix theory. Additionally, we introduce two $n \times n$ dimensional phenomenological random matrix models in which, depending upon crossover parameters, the fluctuation properties measured by the complex spacing ratios show an interpolation between 1D-Poisson to GinUE and 2D-Poisson to GinUE behaviour. Here 1D and 2D Poisson correspond to real and complex uncorrelated levels, respectively.

I. INTRODUCTION

Non-hermitian hamiltonians possessing complex eigenvalues arise in a wide variety of systems such as those with dissipation: the dissipative kicked rotor, open quantum systems such as boundary driven spin chains containing spin injection/ejection terms or gain-loss type hamiltonians popularly found in quantum optics. Among non-hermitian hamiltonians, a subclass is formed by those which possess the constraint of \mathcal{PT} or the more general \mathcal{RT} symmetry and therefore show real spectra. These hamiltonians have received a lot of attention since real eigenvalues guarantee unitary time evolution leading to conservation of probability amplitude which is fundamental to describing a quantum theory useful in physical interpretation of natural phenomena. The subject of \mathcal{PT} symmetric quantum mechanics has been deeply enriched by the seminal works of Bender, Mostafazadeh and others [1–12] who have established it as an extension of the conventional or Hermitian quantum mechanics.

Mathematically, the linear parity operator \mathcal{P} performs spatial reflection and has the effect $p \to -p$ and $x \to -x$ whereas the anti-linear time-reversal operator \mathcal{T} has the effect of $p \to -p$, $x \to x$ and $i \to -i$. The joint action of \mathcal{PT} together is basically a reflection i.e. $\mathcal{PT} = (\mathcal{PT})^{-1}$. In their works Bender and his co-workers have defined a wide class of non-hermitian \mathcal{PT} -symmetric hamiltonians. In general it has been shown that the reality of quantum spectrum is an outcome of unbroken \mathcal{PT} symmetry. A hamiltonian is called \mathcal{PT} symmetric if its eigenfunctions are simultaneously eigenfunctions of the \mathcal{PT} operator,

and in such cases \mathcal{PT} symmetry is not spontaneously broken. Many examples of non-hermitian hamiltonians possessing \mathcal{PT} symmetry has been discussed in the following Refs [1, 2, 4, 5, 13–25]. Beyond complex hamiltonians with \mathcal{PT} symmetry possessing real spectra, one comes across hamiltonians which are \mathcal{RT} i.e. rotation-time symmetric. It has been demonstrated in Ref [51] that \mathcal{RT} symmetry is a superset i.e. a more general notion compared to \mathcal{PT} , such that a wide class of hamiltonians may be identified that have properties similar to that of \mathcal{PT} -symmetric systems, despite not being explicitly \mathcal{PT} -symmetric (\mathcal{PT} symmetry is only a special class of \mathcal{RT} symmetry).

In many cases, non-hermiticity may be rendered to a system even without making it open in the sense of being in contact with an external bath or environment. For example, by the addition of external imaginary fields, efforts have been made to introduce PT symmetry to achieve reality of spectrum, such as for a Ising model [26]. Besides this many other popular hermitian spin chain models have been modified to include imaginary interactions and therefore show complex spectra. The Ising model in presence of a magnetic field in the z-direction as well as a imaginary field in the x-direction has been studied analytically in Ref. [26]. Therein the authors examine various symmetries of the system and study the spin system in the light of perturbation theory, providing some exact results for magnetization along the z and x directions. This modified Ising model is the discretized lattice version of the Yang-Lee model considered by von Gehlen in Refs. [27, 28]. In fact the Lee-Yang zeros have recently been observed by measuring the quantum coherence of a probe spin coupled to an Isingtype spin bath. The quantum evolution of the probe spin introduces a complex phase factor which effectively realises an imaginary magnetic field. It also substan-

^{*} ayanas1994@gmail.com, (she/her)

[†] sensunidhi96@gmail.com, (she/her)

[‡] skumar.physics@gmail.com, (he/him)

tiates that imaginary magnetic fields are not unnatural and are indeed experimentally accomplishable [52]. The classical Heisenberg spin chain with \mathcal{PT} symmetry has been studied under the action of Slonczewski spintransfer torque modeled by applying an imaginary magnetic field [53]. Interestingly this correlation between the imaginary magnetic field on spin dynamics and Slonczewski spin-transfer torque allows an experimental verification of the \mathcal{PT} symmetry-breaking phase transition in some spin chains [29, 30]. Exact solutions using the Bethe ansatz technique has been given for an XXZ spin chain in the presence of an imaginary magnetic field at the boundary in Ref. [31]. Such exact solutions are also available for the one-dimensional dissipative Hubbard model with two-body loss [32]. Giorgi in Ref. [33] has studied spontaneous PT-symmetry breaking in an exactly solvable non-hermitian dimerized chain where non-hermiticity is introduced via a staggered magnetic field. In Ref. [34] a PT-symmetric non-Hermitian version of a quantum network originally proposed in Refs. [35, 36] has been studied in the context of quantum state transfer. Besides the above examples, non-hermiticity may also arise from \mathcal{PT} symmetric on-site imaginary potentials in tight-binding models and strongly correlated systems [37–48]. \mathcal{RT} symmetric bosonic and fermionic systems have been studied in various capacities in Refs. [49–51]. Some authors have focused on fermionic spin chains, for example in Refs. [49, 50], Zhang and Song have analytically studied and identified exceptional points and regions of broken as well as unbroken symmetries in an one-dimensional anisotropic non-hermitian XY model in transverse magnetic field (z-direction) having intrinsic \mathcal{RT} -symmetry, with respect to certain parameters.

Despite such wide analytical exploration, hermitian spin chains of the above kind have remained more or less unexplored in the framework of random matrix theory and quantum chaos. We aim to fill this gap by studying the short range fluctuation properties of the anisotropic XY model in a transverse magnetic field (z-direction) having intrinsic \mathcal{RT} -symmetry introduced by Zhang and Song in Ref. [49]. Along with this, the above hamiltonian is modified to add a longitudinal magnetic field along the x-direction. On addition of this field, an integrability to quantum chaotic transition is observed, portrayed by a symmetry crossover from Poisson to GinUE-resembling statistics of RMT. This is one of the key results of this work. In another highlight, we consider two n-dimensional phenomenological random matrix models in which, depending upon crossover parameters α and δ respectively, the fluctuation properties show transition between 1D-Poisson to GinUE and 2D-Poisson to GinUE behaviour. By 1D and 2D Poisson we mean real and complex uncorrelated levels, respectively. Additionally, we study the spectral fluctuation for the same spin chains by making the transverse field imaginary in presence of the longitudinal magnetic field. The eigenvalues of both these hamiltonians are complex in nature and the complex spacing ratios along with the corresponding radial and angular marginal distributions have been used to quantify the fluctuation properties. This kind of parameter-dependent spectral transition has already been observed and studied exhaustively in several many body quantum systems such as spin chains, lattice models and periodically driven systems [54–62].

The organisation of this paper is as follows. This introduction section is followed by Sec. II wherein the complex spacing ratios and related concepts have been recalled. We discuss the interpolating matrix models in Sec. III followed by the investigated spin hamiltonians in Sec. IV. Sec. V contains a discussion of the significant results. We conclude with a summary of major results along with possible future directions in Sec. VI.

II. COMPLEX SPACING RATIOS

The complex spacing ratios (CSR) introduced in Ref. [64] have come up as a reliable measure for exploring the fluctuations properties of complex spectra. It may be defined for both real and complex spectra and may or may not coincide with any of the popular ratio distributions like the normal spacing ratios [65–68] and the NN-NNN ratios [69]. We briefly recapitulate the techniques involved in finding CSR, for completeness of the paper.

Let $\{x_1, x_2, \dots, x_n\}$ denote real or complex eigenvalues. For each eigenvalue x, x^{NN} denotes the nearest neighbor while x^{NNN} is the next-nearest neighbour identified on the basis of distances in real or complex plane (\mathbb{R} or \mathbb{C}). The CSR are then defined as,

$$z_k = \frac{x_k^{NN} - x_k}{x_k^{NNN} - x_k}. (1)$$

When the spectrum is real, $z \equiv r$ with $-1 \le r \le 1$. On the other hand for complex spectra, $z = a + ib = re^{i\theta}$, where $0 \le r \le 1$. Besides the density plot for the ratios, the radial $P(r) = \int\limits_0^{2\pi} d\theta r \rho(r,\theta)$ and the angular

 $P(\theta) = \int_{0}^{\infty} dr r \rho(r, \theta)$ marginal distributions are also considered. Furthermore, along with the density of CSR and the corresponding marginal distributions, it is important to look at the averages of these quantities, i.e. $\langle r \rangle$ and $\langle \cos \theta \rangle$ in order to estimate the parameter value at which such a transition is seen for the particular system and also to get some idea about the underlying symmetry class. Average quantities have already been considered for the normal spacing ratios and they have been helpful in deciding a critical value of the crossover parameter at which the transition from one symmetry class to the another takes place [68]. For uncorrelated eigenvalues/energy levels showing Poisson type spectral fluctuation properties. a flat distribution in the unit circle is observed such that $\rho(z) = (1/\pi)\Theta(1-|z|)$. Consequently the radial and angular distributions are given by $\rho_{poi}(r) = 2r\Theta(1-r)$,

and $\rho_{poi}(\theta) = 1/2\pi$, i.e. $\langle \cos \theta \rangle = \int_{0}^{2\pi} d\theta \cos \theta = 0$. On the

contrary, quantum chaotic behaviour is inferred from an overlap with the Ginibre unitary statistics of random matrix theory featured by cubic level repulsion, $\rho_{GinUE} \propto r^3$ along with a dip in the ratio density at the centre and at small angles. For uncorrelated levels, $\langle r \rangle = 2/3 = 0.66$, while for GinUE/TUE, it is numerically evaluated to be around 0.73. Whereas $-\langle\cos\theta\rangle=0$ for Poisson and \sim 0.15 for 3×3 TUE and ~0.24 for large dimensional GinUE matrices. Basically, $-\langle\cos\theta\rangle$ for TUE converges very slowly to the large GinUE results, while this convergence is comparatively faster for $\langle r \rangle$. Thus angular dependence of spectral fluctuations captured via CSR is a definitive signature of dissipative quantum chaos [64].

In Ref. [64] the authors deduce analytical expressions of CSR for hermitian (arbitrary, Gaussian and Circular ensembles) and non-hermitian ensembles like the 3×3 case of the Ginibre Unitary and that for the Toric ensembles are expressed in the form of a N-1 integral which can be evaluated numerically. The 3×3 results for GinUE are not universal in nature and does not approximate large-N behaviour whereas the N-general results of TUE well approximates large N behaviour and has been used in several contexts. Recently, exact expressions of CSR for the Ginibre Unitary ensembles in the large N limit has also been deduced [72]. Since its formulation, the complex spacing ratios have found applications in a wide variety of quantum systems [70–72].

III. PHENOMENOLOGICAL MATRIX MODELS FOR POISSON-GINUE CROSSOVER

For a system making a transition from integrable to chaotic dynamics, the spectral fluctuation properties, typically measured by the distribution nearest neighbour spacings and their ratios show a crossover from Poissonian to a random matrix ensemble of appropriate symmetry class. In this regard, interpolating formulas for the ratios of spacings of consecutive eigenvalues for Poisson-GOE, Poisson to semi-Poisson transitions and several exact results pertaining to crossover ensembles like GOE-GUE, GSE-GUE are already well known in RMT [63, 68, 75–77]. On the other hand, transitional models or crossover ensembles have remained far less explored in non-hermitian systems and non hermitian RMT. A few examples can be found in the following Refs. [78-81]. In this section we consider some phenomenological $n \times n$ interpolating random matrix ensembles to model the integrable-quantum chaotic transition in non-hermitian systems. At first a hamiltonian ensemble interpolating between 1D Poisson (real uncorrelated entries in the hamiltonian) and the GinUE (matrix model 1: MM1) given below,

$$H_{\alpha}^{(1)} = \frac{H_0^{(1)} + \alpha V}{\sqrt{1 + \alpha^2}},\tag{2}$$

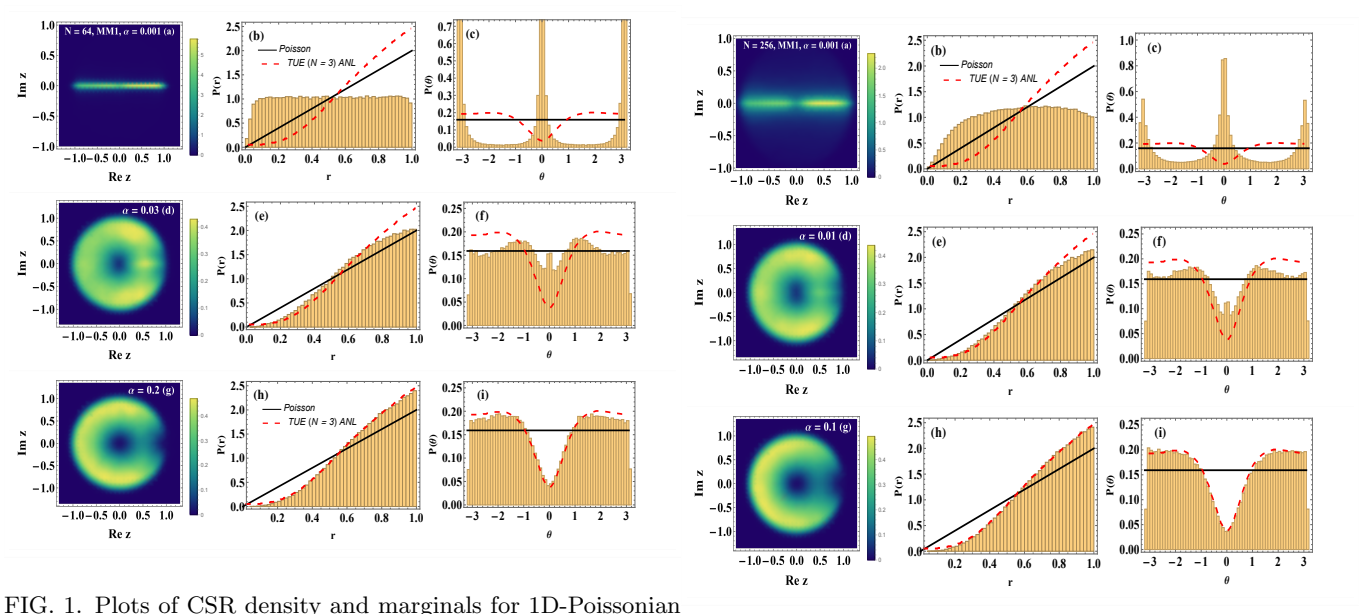
 $H_0^{(1)}$ is chosen such that it is a $n \times n$ diagonal matrix with $(H_{00})_{ii}^{(1)}$, $i=1,2,\cdots,n$ entries being independent, real, zero-mean, unit-varianced Gaussian variables while V is chosen as a matrix from GinUE i.e. the matrix elements are complex, i.i.d Gaussian variables with zero-mean and unit-variance. In this case when $\alpha=0$ we get $H_0^{(1)}$ which has all real entries and the corresponding eigenvalues are also real and at $\alpha\to\infty$, V is obtained. As alpha is increased, intermediate statistics starts to show and the eigenvalue spectra becomes complex and the imaginary parts of the eigenvalue becomes significant. This is also reflected in the complex spacing ratios which have been plotted and discussed below.

In another related model, an ensemble interpolating between 2D-Poisson (complex uncorrelated entries in the hamiltonian) and the GinUE (matrix model 2 : MM2) given below,

$$H_{\alpha}^{(2)} = \frac{H_0^{(2)} + \alpha V}{\sqrt{1 + \alpha^2}}.$$
 (3)

Here $H_0^{(2)}$ is a $n \times n$ diagonal matrix with $(H_{00})_{ii}^{(2)}$, $i=1,2,\cdots,n$, being independent complex, zero-mean, unit-varianced Gaussian variables while V is a GinUE matrix. When $\alpha=0$ we get $H_0^{(2)}$ and at $\alpha\to\infty$ we get V. Here, the eigenvalue spectra is complex and CSR density is either uniform in the unit circle or shows standard features of GinUE depending upon the crossover parameter.

We study the CSR density and the corresponding marginals for the above discussed ensembles by tuning the interpolation parameter α . For MM1 i.e. 1D-Poisson to GinUE, plots of matrix dimensions N=64 and 256 with ensemble comprising 3000 and 1500 matrices, respectively, are presented in Figs. 1 and 2. The results from matrix model simulation has been represented with the histogram whereas the black solid and red dashed lines respectively correspond to Poisson and TUE analytical results of marginal densities of CSR. The stark differences between the top rows (a-c), for $\alpha = 0.001$ in the above mentioned figures with the rest of the plots (for higher values of α) is due to the real eigenvalue spectra of corresponding hamiltonian having either very small or zero imaginary parts. This is the reason an accumulation of CSR on the real line is noted for $\alpha = 0.001$ which gradually tend to spread in the unit disc (GinUE-like statistics) for higher values of α . For MM2, 2D-Poisson to GinUE, the plots are presented in Figs. 3, 4 and 5 for matrix dimensions N = 64, 256 and 2000 with corresponding ensemble sizes of 3000, 1500 and 100 each respectively. In Fig. 4, for relatively smaller matrix dimensions (N=256), at the Poissonian limit $(\alpha=0)$, although CSR density and P(r) matches closely with the expected Poissonian analytical results, the angular marginal distribution shows elevated density close to the origin ($\theta = 0$). This is due to small matrix size and becomes nearly uniform once the dimension is further increased to N = 2000 in Fig. 5.



to GinUE crossover in MM1 for 3000 matrices of size N=64. In MM1, the random diagonal matrices have real Gaussian entries FIG. 2. In this case the same plots for MM1 are presented for along the diagonal.

an ensemble of 1500 matrices of dimension N=256.

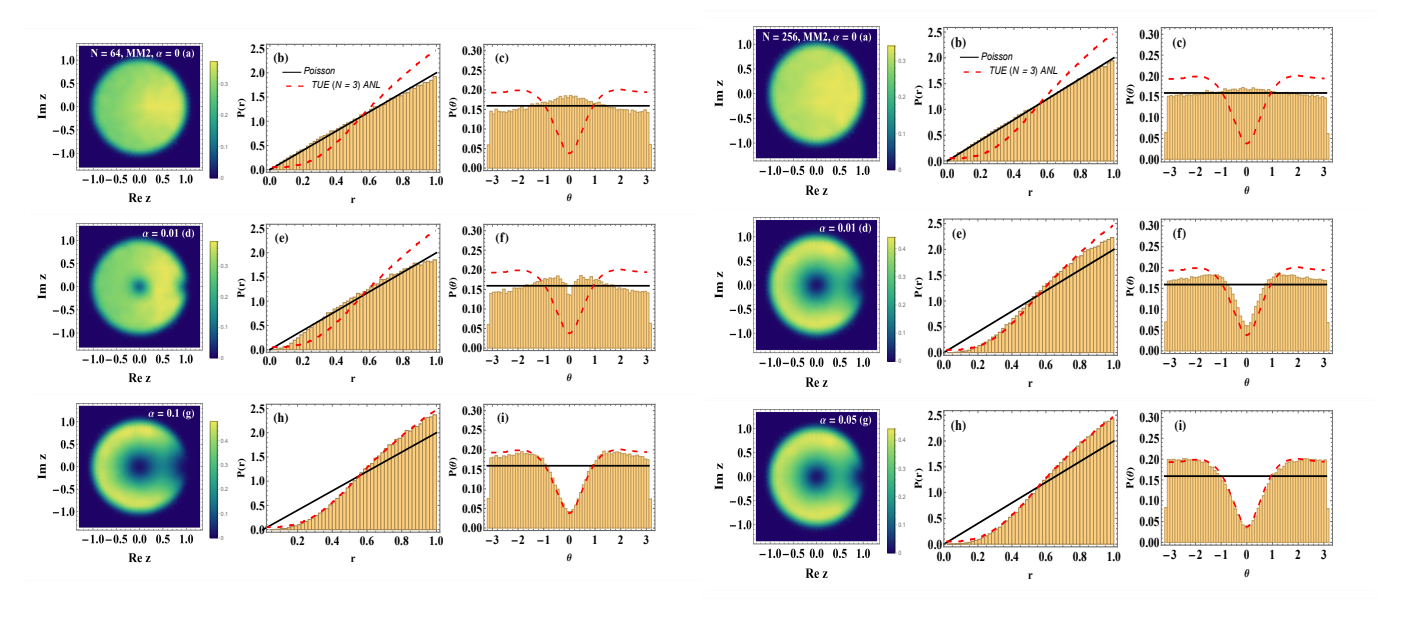


FIG. 3. 2D-Poissonian to GinUE crossover for MM2 seen from the density of CSR and marginals for an ensemble of 3000 ma- FIG. 4. 2D-Poissonian to GinUE crossover for MM2 seen from the density of CSR and marginals for an ensemble of 1500 matrices of dimension N=64.

IV. INVESTIGATED HAMILTONIAN MODELS

An XY model in the presence of a transverse magnetic field (field along z-direction) may be represented as,

$$H^{(XY)} = \sum_{j=1}^{L} \left(J_x \sigma_j^{(x)} \sigma_{j+1}^{(x)} + J_y \sigma_j^{(y)} \sigma_{j+1}^{(y)} + \lambda \sigma_j^{(z)} \right), \quad (4)$$

where J_x and J_y are the coupling constants while λ is the strength of the field along the z-direction. The coupling constants for the Heisenberg terms may be modified to introduce imaginary ones, creating a non-Hermitian version of the above, as given below [49],

$$H_1 = \sum_{j=1}^{L} \left(\frac{1+i\gamma}{2} \sigma_j^{(x)} \sigma_{j+1}^{(x)} + \frac{1-i\gamma}{2} \sigma_j^{(y)} \sigma_{j+1}^{(y)} + \lambda \sigma_j^{(z)} \right),$$
(5)

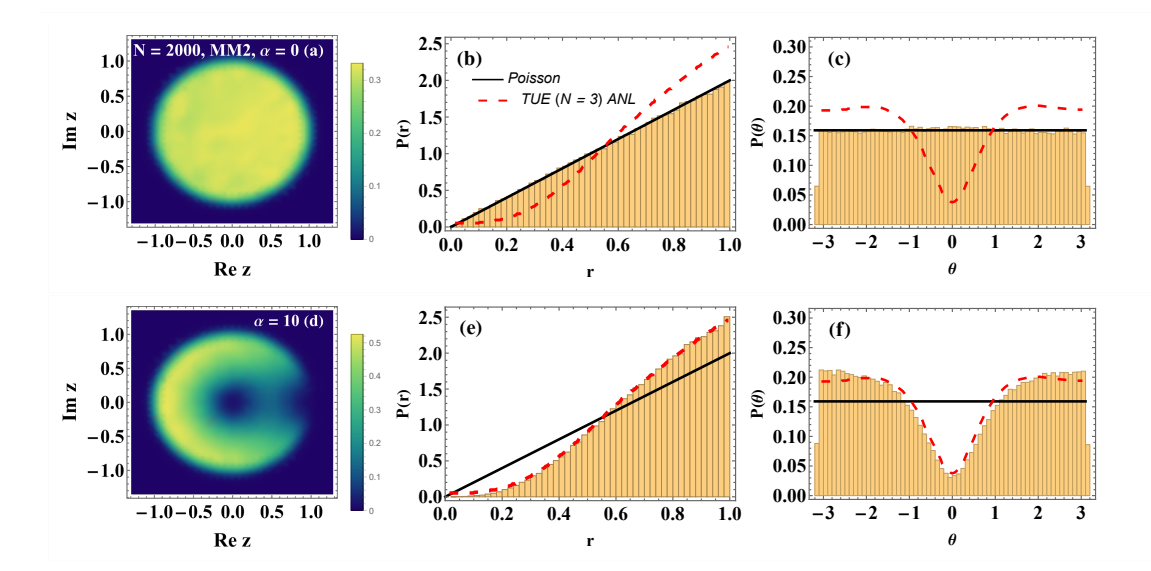


FIG. 5. Density of CSR and marginals for an ensemble of 100 matrices of size N=2000 in the MM2 matrix model for various values of α . When $\alpha=0$, Poissonian distribution is obtained while for larger values of α , say 10, results matching well with N=3 analytical TUE results. Flat distribution at small angles and origin is seen as expected for

where we have set $J_x = J_y = 1$. The parameter γ controls the non-hermiticity whereas λ is the strength of the magnetic field along the z-direction, such that λ and $\gamma \in \mathbb{R}$. The operators $\sigma^{(x,y,z)}$ act on a $(\mathbb{C}^2)^{\otimes L}$ dimensional Hilbert space, L being chain length. In terms of $2^L \times 2^L$ Pauli matrices and identity matrices these are given by, $\sigma_i^{(x,y,z)} = \mathbb{I} \otimes \mathbb{I} \otimes \otimes \sigma^{(x,y,z)} \otimes ... \otimes \mathbb{I} \otimes \mathbb{I}$. The Pauli matrix part acts on the *i*th site of the chain while the identity operator I acts on the rest of the sites. Periodic boundary conditions are chosen such that $\sigma_{N+1}^{(x,y,z)} = \sigma_1^{(x,y,z)}$. In Ref. [49], the authors have exactly solved this spin chain model using the standard techniques of Jordan-Wigner, Fourier and Boguliobov transformations extended to complex versions. Based on the exact results, exceptional points separating brokenunbroken regions of symmetry have also been identified. H_1 has full real spectrum since it commutes with the \mathcal{RT} operator, $[\mathcal{RT}, H_1] = 0$ and therefore share the same set of eigenvectors with \mathcal{RT} [49]. The operator \mathcal{R} is the linear rotation operator and has the effect of rotating each spin by an angle of $\pi/2$ about the z-axis i.e. the xy plane,

$$\mathcal{R} \equiv \exp\left[\frac{i\pi}{4} \sum_{i=1}^{L} \sigma_i^{(z)}\right] = \prod_{i=1}^{L} \frac{1}{\sqrt{2}} (\mathbb{I} + i\sigma^{(z)})_i. \quad (6)$$

This amounts to an action : $(\sigma_i^{(x)}, \sigma_i^{(y)}, \sigma_i^{(z)}) \rightarrow (-\sigma_i^{(y)}, \sigma_i^{(x)}, \sigma_i^{(z)})$. A hamiltonian symmetric with respect to an anti-linear operator such as \mathcal{T} , shows eigenvalues which are either real or appear in complex conjugate pairs [6, 7]. Generally in quantum mechanics and field theories the \mathcal{PT} symmetry is taken to be anti-linear operator which carries out a simultaneous parity transformation $\mathcal{P}: x \to -x$ and time reversal $\mathcal{T}: t \to -t$. When

acting on the Pauli matrices, \mathcal{T} acts as a complex conjugation such that $(\sigma_i^{(x)}, \sigma_i^{(y)}, \sigma_i^{(z)}) \rightarrow (\sigma_i^{(x)}, -\sigma_i^{(y)}, \sigma_i^{(z)})$. Two limiting cases of the above hamiltonian are of particular importance. Firstly when $\gamma = 0$, the above hamiltonian reduces to the ordinary XY model with an external magnetic field in the z direction, the $J_x = J_y = 1$ case of Eq. (4).

$$H_0 = \frac{1}{2} \sum_{j=1}^{L} \left(\sigma_j^{(x)} \sigma_{j+1}^{(x)} + \sigma_j^{(y)} \sigma_{j+1}^{(y)} + 2\lambda \sigma_j^{(z)} \right). \tag{7}$$

 H_0 is left unchanged under the action of \mathcal{R} and \mathcal{T} separately as well us under their joint action. However for the hamiltonian H_1 , $[\mathcal{R}, H_1] \neq 0$ and $[\mathcal{T}, H_1] \neq 0$ but $[\mathcal{RT}, H_1] = 0$. In the other limiting case of H_1 when $\gamma >> \lambda$ or 1, H_1 reduces to

$$H_{im} = \frac{i\gamma}{2} \sum_{i=1}^{L} \left(\sigma_j^{(x)} \sigma_{j+1}^{(x)} - \sigma_j^{(y)} \sigma_{j+1}^{(y)} \right)$$
(8)

displaying a fully imaginary spectrum. Any eigenstate of H_{im} corresponding to any non zero eigenvalue is not an eigenstate of the \mathcal{RT} operator. In the above model \mathcal{RT} symmetry plays the same role as \mathcal{PT} symmetry does in the generally studied \mathcal{PT} -symmetric pseudo-Hermitian systems showing real spectrum [1, 2]. We modify H_1 by adding a random field along the x-direction

$$H_{2} = \sum_{j=1}^{L} \left(\frac{1+i\gamma}{2} \sigma_{j}^{(x)} \sigma_{j+1}^{(x)} + \frac{1-i\gamma}{2} \sigma_{j}^{(y)} \sigma_{j+1}^{(y)} + \lambda \sigma_{j}^{(z)} + \lambda_{1} \sigma_{j}^{(x)} \right). \tag{9}$$

The introduction of this perturbative longitudinal field makes H_1 non-integrable on proper tuning of the system parameters like γ , λ and λ_1 . It also breaks the \mathcal{RT} invariance of the system. Specifically when the x-field is random and the z-field is varied manually we see signatures of integrability, breaking portrayed by a transition from Poisson to Ginibre unitary statistics. In fact the general trend remains the if instead of $\sigma_j^{(x)}$, one introduces the $\sigma_j^{(y)}$ field. Another variant of the above model is one where the z-field is imaginary

$$H_{3} = \sum_{j=1}^{L} \left(\frac{1+i\gamma}{2} \sigma_{j}^{(x)} \sigma_{j+1}^{(x)} + \frac{1-i\gamma}{2} \sigma_{j}^{(y)} \sigma_{j+1}^{(y)} + i\lambda \sigma_{j}^{(z)} + \lambda_{1} \sigma_{j}^{(x)} \right). \tag{10}$$

The significance of such imaginary fields have already been discussed in Section I. However this field makes the eigenvalues complex having a significant imaginary part even when γ is small, since now the paramater λ also contributes to complex eigen-energies. For this hamiltonian, the transition from integrable to chaotic dynamics maybe modeled by matrix model 2 introduced earlier. This is expressed in the density of the CSR, which spreads over the whole unit disc, when γ is very small. In the two previous hamiltonians, H_1 and H_2 , this was not the case since γ was the only non-hermiticity inducing parameter.

V. EMPIRICAL RESULTS : DISCUSSION

In this section we discuss the results of short range spectral fluctuation properties of the above discussed non-hermitian spin chain hamiltonians using the complex spacing ratios in which quantum chaotic behaviour can be identified via its vanishing density at the origin and a suppression of the same at small angles. This suppression of small angles is seen in the angular marginal distribution $P(\theta)$ and the slightly undulatory nature of the radial marginal distribution P(r) is due to the cubic level repulsion distinctive of the Ginibre ensembles, the non-hermitian analog of the Gaussian ensembles. One of our key observations is the Poisson to GinUE/TUE like spectral transition for certain range of parameters in H_2 and H_3 studied for chain lengths of L=6 and 8. Through our numerical experiments we identify parameter values for which these spin systems show statistics quite similar to a transition from Poisson to the N=3 exact Toric unitary ensemble (TUE) results which approximates well the large-N statistics of the Ginibre Unitary ensemble (GinUE) of random matrices.

The plots appended later in this section contains results of density of CSR, P(r) and $P(\theta)$ for all the three hamiltonians H_1 , H_2 and H_3 prepared by varying parameters controlling non-hermiticity and strengths of the magnetic fields. For each of the cases, one of the parameter for each set is changed manually while the others are

chosen to be zero-mean, unit-variance Gaussian random numbers $(\in \mathcal{N}[0,1])$. The whole spectrum of eigenvalues are considered for generating these results. The overall size of the Hilbert spaces or hamiltonian matrices corresponding to L=6 and L=8 sized spin chains are 64 and 256 respectively. An ensemble 4000 and 1500 matrices are considered respectively for each of the chain lengths and various statistical properties of the energy spectra are examined. Even for moderate chain lengths (L = 6) on properly adjusting system parameters the results are quite close to those from the TUE. For the H_2 hamiltonian the integrability breaking and transition from Poisson to RMT statistics is quite clear. In general, a rich variety of spectral behaviour is observed for all the three hamiltonians as the parameters are varied. The results for each hamiltonian is discussed in greater detail in the subsequent subsections.

A. Plots for H_1

Here we study the spectral properties of H_1 . In Fig. 6 the spectral fluctuation properties for L=6 of this model is inspected with the variation of γ while $\lambda \in \mathcal{N}[0,1]$. In Fig. 6(a) at $\gamma = 0.01$, only a few complex eigenvalues are seen with either small or negligible imaginary components. This causes the CSR to be spread on the real line or very close to it. In Fig. 6(b) for $\gamma = 0.3$ a very faint density is seen along the real line and this density becomes more pronounced for $\gamma = 2$ in Fig. 6(c) and a bow-arrow like structure is noticed. On inspection of the eigenvalue spectra for this particular case, a number of interesting patterns in the eigenvalues are observed. The eigenvalue spectra contains eigenvalues of the form $\pm a \pm ib$. Besides these complex eigenvalues, there are real eigenvalues which have very small imaginary parts and some of these real eigenvalues are of the form -a and a. These patterns of the eigenvalue spectra are also reflected in the CSR distribution which are of $a \pm ib$ structure and degenerate in nature. In Fig 7, CSR density plots along with marginal densities P(r) vs r and $P(\theta)$ vs θ are plotted. Here λ is varied and $\gamma \in \mathcal{N}(0,1)$. The density plots show some resemblance to Poisson-like statistics in all three cases of $\lambda = 0.01$ in (a)-(c), 0.5 in (d)-(f) and 1 in (g)-(i). There is some increased density of ratios at the centre which becomes more concentrated and hence brighter as λ is increased. In Figs. 7 (c), (f) and (i) the $P(\theta)$ vs θ plot shows uneven surface due to these regions. Unlike $P(\theta)$, P(r) closely follows Poisson statistics (Figs. 7 (b), (e), and (h)). However if λ is increased further the results start showing deviation from the expected Poisson

In some works related to the study of many-body localization transition in non-hermitian models this transition from real to complex eigenvalues and the suppression of imaginary parts of complex eigenenergies for general non-Hermitian hamiltonians having time-reversal symmetry has been discussed as a signature of many-body localiza-

γ	$\langle r \rangle$	$-\langle\cos\theta\rangle$
0.01	0.478661	0.052861
0.3	0.600388	-0.06899
2	0.632759	-0.05897
λ	$\langle r angle$	$-\langle\cos\theta\rangle$
$\frac{\lambda}{0.01}$	$\langle r \rangle$ 0.655424	$-\langle \cos \theta \rangle$ -0.07226
	. ,	
0.01	0.655424	-0.07226

TABLE I. Single number signatures of the $H_1, L = 6$ for parameter values corresponding to the plots.

tion [74].

Besides the plots we provide in Table. I a list of single number signatures $\langle r \rangle$ and $-\langle \cos \theta \rangle$ for various values of λ and γ in. On top of the marginal distributions, the average quantities help in stipulating the exact nature of the distribution and how close it is to being Poisson or GinUE. We see that for H_1 , the average of $\langle r \rangle$ are closer to the values for Poisson i.e. 0.66 and the corresponding $-\langle \cos \theta \rangle \sim 0$. as the values of λ or γ are increased while the other is $\in \mathcal{N}[0,1]$. Numerically, it is seen that these numbers depend on ensemble size to a great extent and this dependence is expected to reduce with larger chain lengths.

B. Plots for H_2

Now we examine the variation in spectral fluctuations for H_2 depending on system parameters γ , λ , and λ_1 . These are shown in Figs. 8, 9 and 10. In Fig. 8, CSR density, P(r) and $P(\theta)$ are studied for three values of $\gamma =$ 0.01, 0.5 and 3. For $\gamma = 0.01$, the spectra exhibits fewer complex eigenvalues as in Fig. 6 (a) with small imaginary parts which reflects in the ratio density spreading on the real line. This is more pronounced on the negative real axis and almost disappears at the origin. For $\gamma = 0.5$ in Figs. 8(d)-(f), in the density plot, quantum chaotic behavior is somewhat evident from the vanishing density at the origin and at small angles. However neither P(r)nor $P(\theta)$ are close to analytical results. In Fig. 8(f) slight dip at small angles is noticed. As the value of γ is further increased, ratio density gets localised at random areas in the unit circle P(r) and $P(\theta)$ show statistics quite distinct from either Poisson or TUE. By carefully tuning λ , it is possible to achieve the best overlap with RMT statistics.

For $\lambda = 0.001$ which corresponds to weak z-field, close-to-Poisson like statistics is observed for the CSR density in Fig. 9(a), a slight dip is noticed in the angular marginal distribution in Fig. 9(c) owing to the slightly lower density of CSR at the centre of the unit circle. However P(r) in Fig. 9(b) matches Poisson statistics closely. The suppression of CSR density at small angles and origin as in

Fig. 9(d), results from an increase in λ to 0.9 and causes clear transition from almost-Poisson to TUE-like statistics. In this case, both marginal densities in Figs. 9 (e) and 9(f) agree with TUE analytics approximately. As λ is raised further, the density of smaller angles increase in the angular distribution : Fig. 9 (i), which is consistent with the accretion of CSR at small angles relative to the rest of the circle in Fig. 9(g). This is exactly the opposite of TUE results.

For H_2 changes in λ_1 also leads to a symmetry transition from Poisson to TUE, which is shown in Fig. 10. Nevertheless, the quantum chaotic features of the TUE ensemble are not as pronounced as in Fig. 9. The overall trend for these plots are similar to that in Fig. 9. Interestingly, although $P(\theta)$ changes significantly as λ_1 is raised, P(r) barely changes and follows almost Poissonian statistics. These findings substantiates that density of CSR and the corresponding marginals provide a reliable technique to study chaotic or integrable dynamics in non-hermitian systems and are able to identify the signatures of quantum chaos. The same plots are also studied for L=8 of the same spin chain in Figs. 11, 12, 13.

In Fig 11, for very small values of $\gamma (= 0.01)$, the ratios again assemble near the real line but eventually spreads across the unit disc. This feature is common for all the cases of γ variation which indicates that this parameter leads to a transition from real to complex eigenvalues. As previously discussed, this kind of transition from real to complex eigenvalues have been indicated in other nonhermitian spin chains models. The TUE-like behavior persists for $\gamma = 2.1$ where for $H_2, L = 6$ on the other hand, the GinUE-like features were not at all prominent. This prominence in quantum chaotic features is due to increased matrix dimension. As γ is increased further, CSR gets localised at certain regions of the unit circle, quite different from either Poisson or TUE behaviour. In Figs. 12(a)-(c), Poisson-like characteristics are noticeably prominent for $\lambda = 0.01$, although a suppression for small angles is seen in $P(\theta)$. For $\lambda = 1.2$, RMT correspondence is well evident. However on inspection it was seen that same as H_2 , chaotic nature begins to disappear and erratic behavior creeps in as λ is further increased. The plots in Fig. 13 show trend similar to that in Fig. 10, however TUE behaviour is much stronger for the latter.

The results for this model can be well approximated by matrix model 1 interpolating between the 1D-Poisson and the GinUE symmetry classes. This overlap can be seen clearly by comparing the plots in Figs. 1 and 2 of the matrix model with that of the hamiltonian in Figs. 8 and 11 and particularly weighing up the cases of $\gamma = 0.01$ and the $\delta = 0.01$. The single number signatures for L = 6 and L = 8 of this chain is given in Tables II and III. We see that for $\lambda = 0.9$, $\langle r \rangle$ is closest to the GinUE value (~ 0.74). These results improve expectedly for L = 8 due to larger matrix dimension. Also negative values of $-\langle \cos \theta \rangle$ in this case and for H_1 seem to be for cases in which the spectral fluctuations are very different from either Poisson or GinUE. Such negative values of $-\langle \cos \theta \rangle$

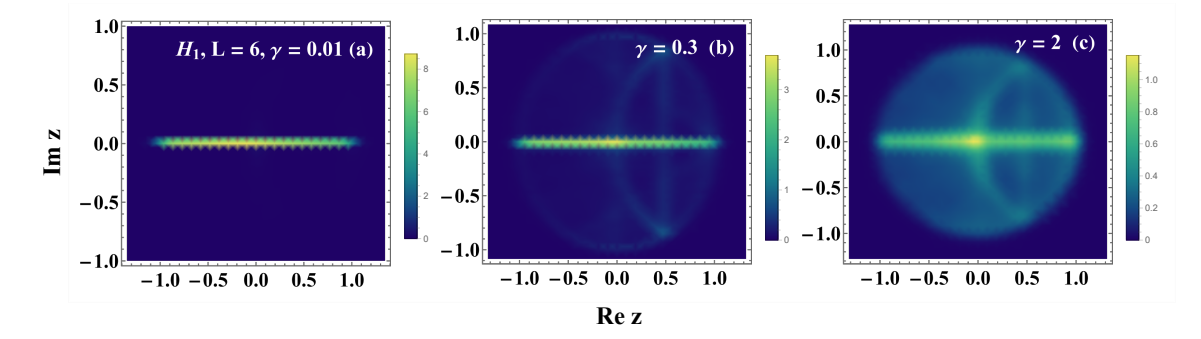


FIG. 6. Plots of density of CSR for L=6 of H_1 . $\lambda \in \mathcal{N}(0,1)$ while $\gamma=0.01, 0.3$ and 2 in (a), (b) and (c). For very low values of γ the densities are distributed on the real axis but they spread out to some extent in the unit disk as the value is increased.

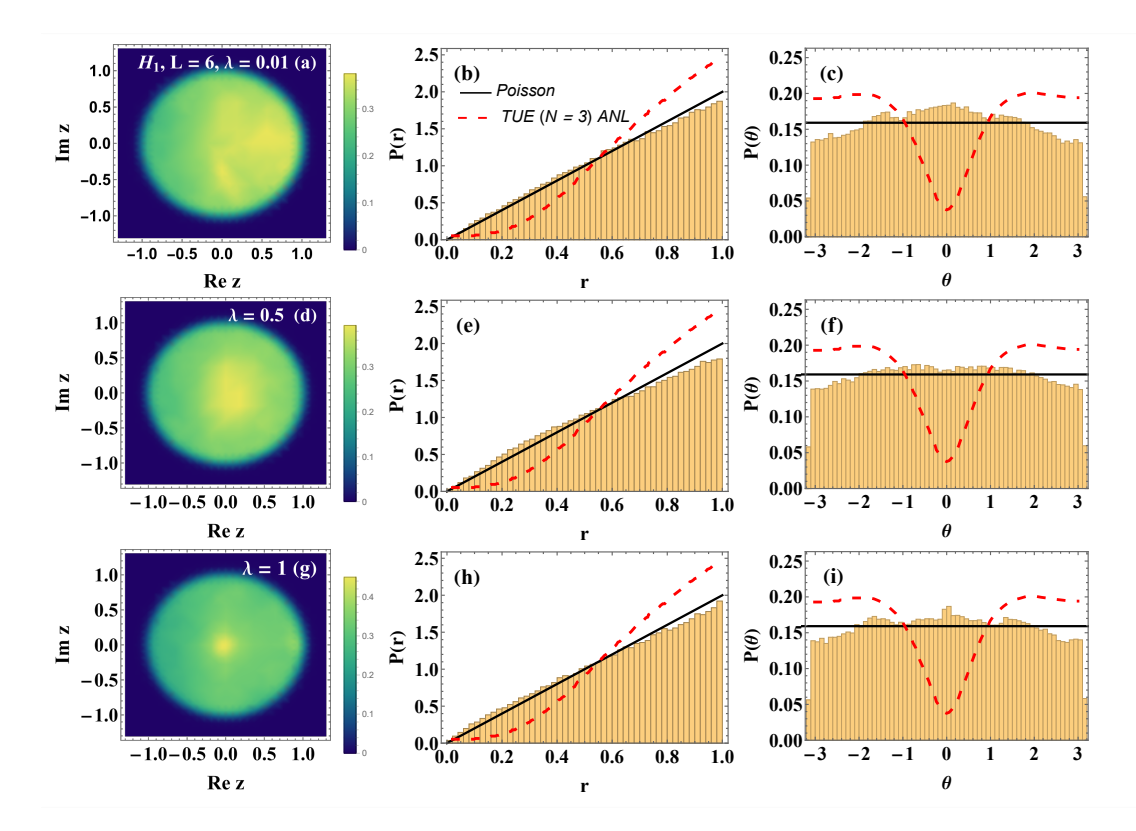


FIG. 7. Plots of CSR density and its marginals (r and θ distributions) for L=6 of the hamiltonian H_1 . The parameters γ are taken as zero-mean unit-variance Gaussian random numbers and λ is chosen as 0.001 for (a)-(c), 0.5 for (d)-(f) and 1 for (g)-(i). Black solid lines depict the analytical results from the Poisson distribution whereas the red one corresponds to the N=3 exact results for the Toric Unitary Ensemble (TUE), which captures well large-N GinUE fluctuation behavior. Fluctuation properties close to Poisson are observed for $\lambda=0.01$ and 0.5, respectively, whereas for $\lambda=1$ the behavior is quite distinct from both these cases.

has also appeared in Ref. [64] for some spin models with bulk dephasing. However further exploration is needed to understand this behaviour in the context of our spin chains.

C. Plots for H_3

For H_3 , we inspect the spectral properties for a chain length of L=8 in Figs. 14,15 and 16. In Fig. 14,

GinUE-like statistics persists till $\gamma=2.2$ however decreases slowly as γ is increased. The non-integrable behaviour persists for larger values of the non-hermiticity parameter, compared to H_2 . For H_3 we show only the results for L=8. As expected on increasing the strength of the parameters, the results deviate significantly from RMT or Poissonian results. The results of this hamiltonian overlaps with the simulations of matrix model 2 interpolating 2D-Poisson to GinUE which becomes evident from comparing the plots in Figs. 4 and 14. For H_3 ,

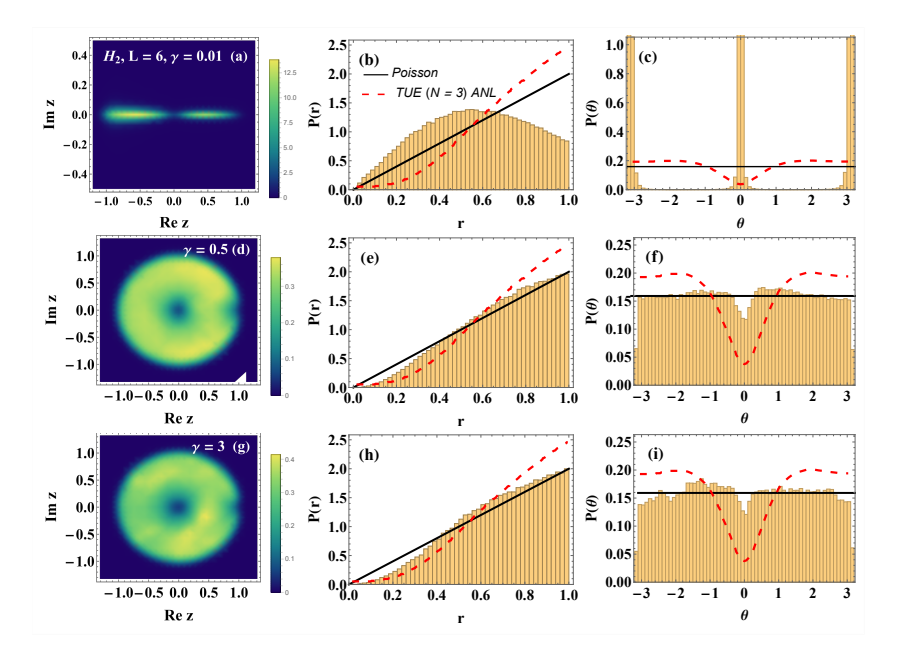


FIG. 8. Plots of CSR density for L=6 of the H_2 hamiltonian with γ varied manually while λ , $\lambda_1 \in \mathcal{N}(0,1)$. $\gamma=0.01$ in (a)-(c)(top row), 0.5 in (d)-(f) (middle row) and 3 for (g)-(i) (bottom row). The plots (d)-(f) show subtle signatures of N=3 exact results for the TUE denoted by the red line. The ratio density at the centre, vanishes to some extent in (d). This is also seen in the $P(\theta)$ vs θ plot in (f) which also shows slight suppression of small angles. For $\gamma=3$ in (g) the results of density plots are sommewhat different with areas of elevated brightness on the disc but the marginals are similar to the previous one.

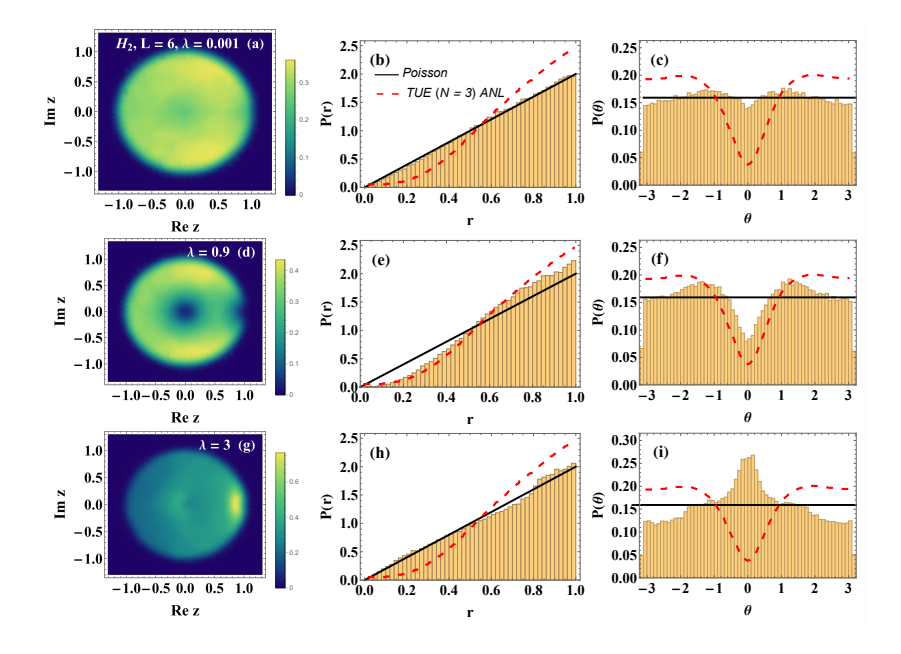


FIG. 9. Plots of CSR and its marginals for H_2 with manual variation of λ , with γ and $\lambda_1 \in \mathcal{N}[0,1]$. Poisson-like behaviour featured by a flat distribution of the ratio density in the unit circle and uniform radial and angular distributions is observed for $\lambda = 0.001$, in (a)-(c) (top row). As the value of λ is increased, large-N GinUE behaviour is observed for $\lambda = 0.9$ in (d)-(f) (middle row). P(r) shows slight undulation, a distinguishing feature in the TUE case. P(θ) on other hand shows a strong suppression of small angles. On the contrary for $\lambda = 3$ in (g)-(i) (bottom row) accumulation of CSR at small angles is observed.

the z-field is imaginary besides the coupling constants and therefore contributes to the complex spectra. As a result, even when γ is small, more or less uniform density of CSR is observed in the unit circle unlike for H_1 or H_2

which for lower values of γ show an accumulation of CSR on the real line. The single number signatures are given in Table IV and for certain values of the system parameters the results are close to GinUE but for most of the

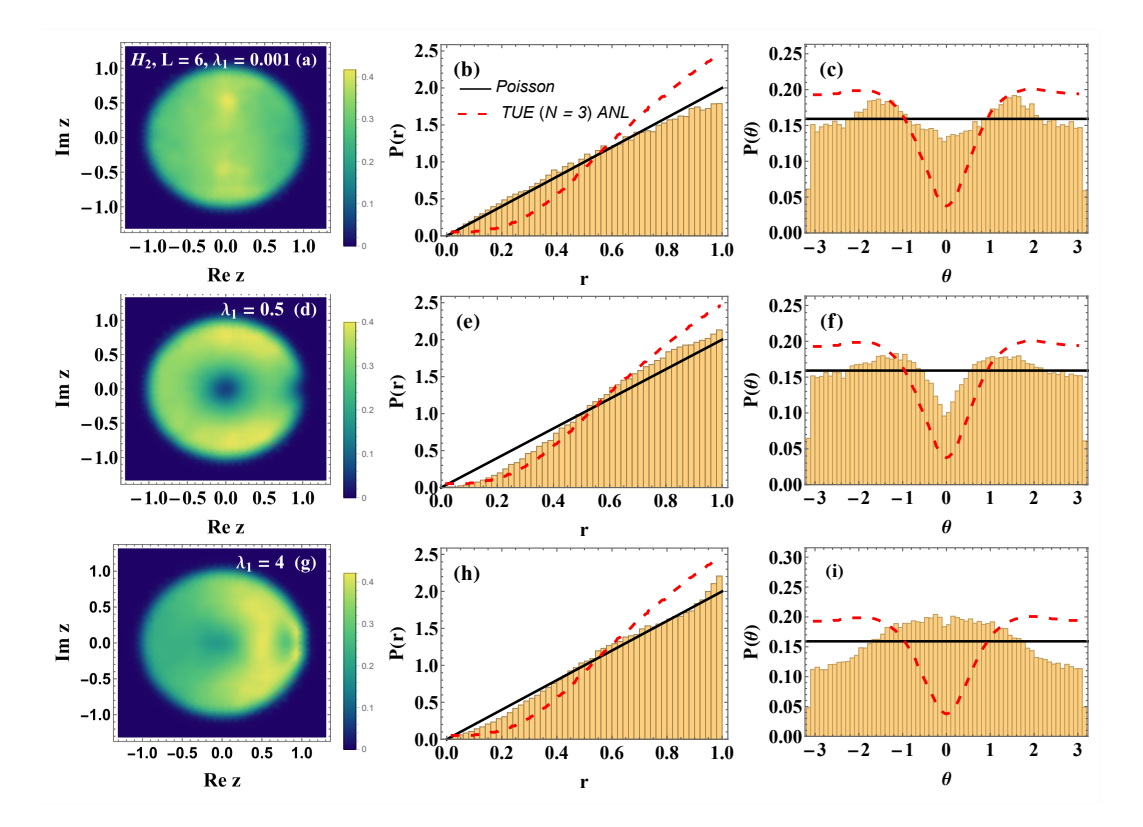


FIG. 10. In this case only λ_1 is varied while the remaining two are random numbers. Although close-to-Poisson behaviour is seen for $\lambda_1 = 0.001$ in (a)-(c) (top row), RMT behaviour is much less prominent when λ_1 as compared to λ being varied.

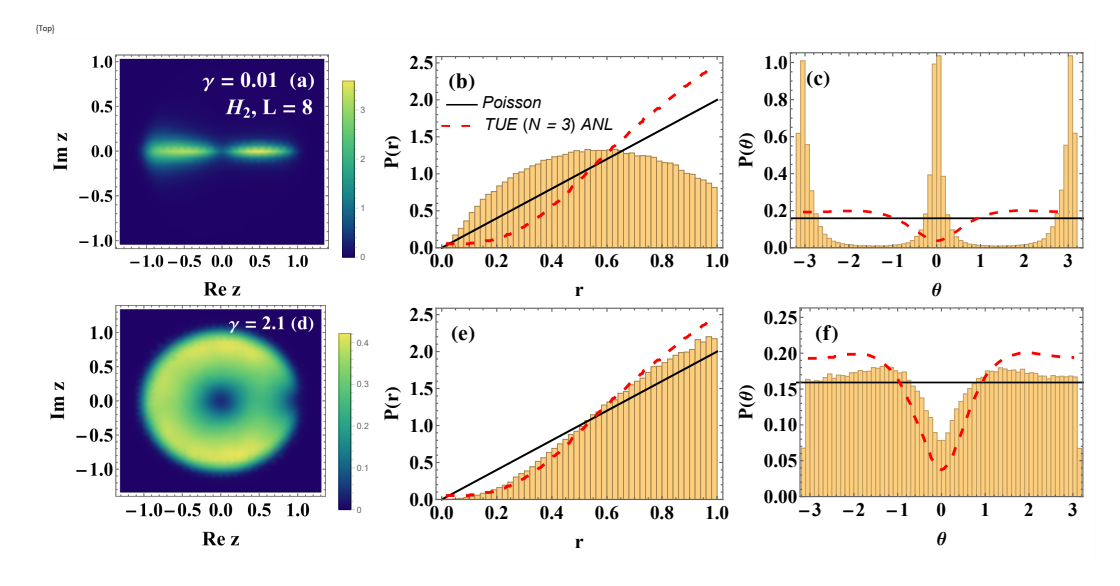


FIG. 11. In this case, the same statistics is investigated for a chain of length L=8 with γ variation. Due to larger chain size, the suppression of small angles is much more prominent and persists for a larger range of values compared to the L=6 case. Especially for $\gamma=2.1$ in (d)-(f), TUE features are still notable.

parameter range they are closer to Poisson-like statistics.

VI. SUMMARY

In this paper we have studied the short range spectral fluctuation properties of three non-hermitian spin chains using complex spacing ratios. The key aspects considered

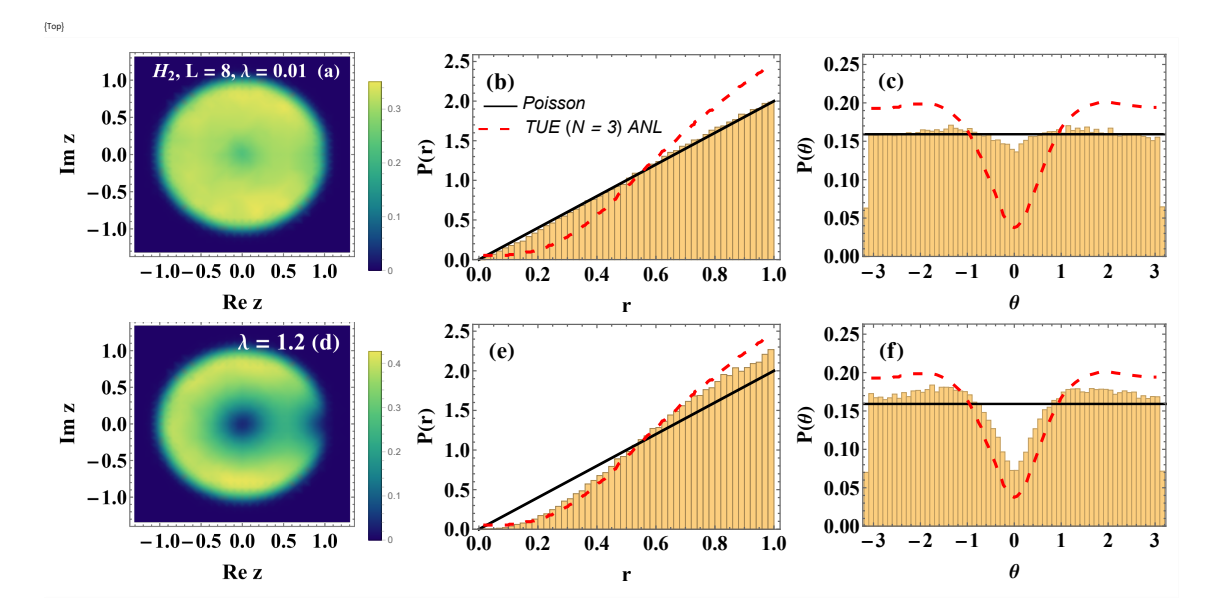


FIG. 12. In this case λ is varied for L=8. Poisson-like features are very prominent for $\lambda=0.01$ in (a)-(c) in the top row and when λ is increased to 1.2 in (d)-(f) (bottom row) the features are close to the analytical results.

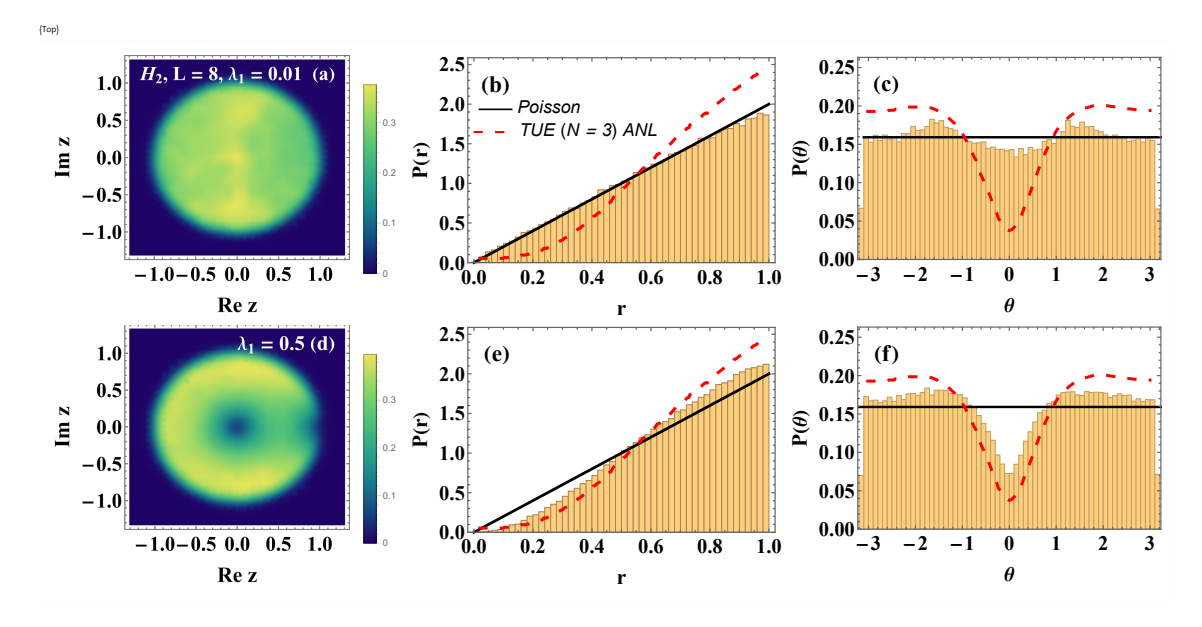


FIG. 13. In this case, λ_1 is varied manually for L=8 of the H_2 hamiltonian. Larger spin chain ensures more prominent RMT behavior for $\lambda_1=0.5$ ((d)-(f), bottom row) compared to the $\lambda_1=0.1$ in L=6 spin chain size.

in this paper can be summarised in the following three points. Firstly, in these spin chains non-hermiticity has been rendered by the addition of complex coupling constants and imaginary random transverse fields. Therefore they are not "open" in that sense, since there is no direct interaction with the environment (which may be a larger spin system) such as in boundary driven spin chains or dissipative ones. Also, this anisotropic non-hermitian XY model has been shown to be \mathcal{RT} symmetric in Ref. [49] which plays the same role as \mathcal{PT} -symmetry does in other pseudo-hermitian spin chain models.

Secondly, the spin chains have been modified by the addition of an extra random longitudinal field (along the x-direction) which leads to integrability breaking and a transition from Poisson to GinUE-resembling statistics of RMT is seen. These studies of integrability breaking and symmetry crossovers due to disorder have been pursued in several hermitian spin chains. For the spectral fluctuation properties and the corresponding single number signatures for which the values are mostly close to Poisson (~ 0.66), it is expected that signatures of non-integrability and overlap with RMT results improve with

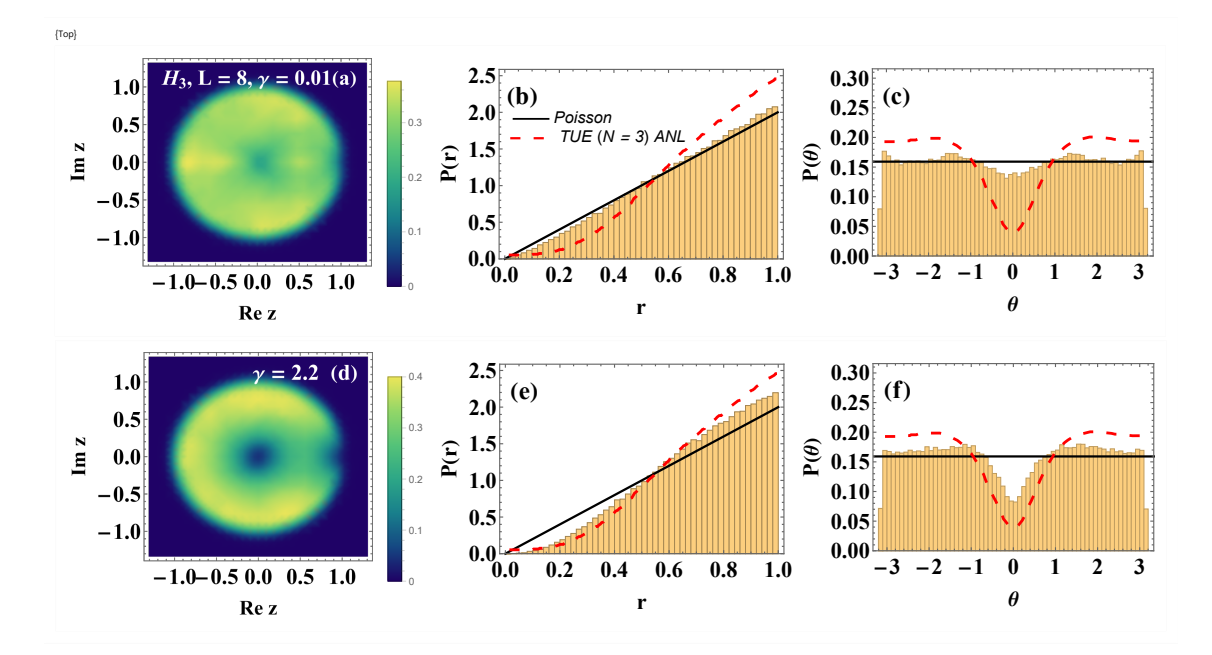


FIG. 14. Same plots for L=8 of the H_3 hamiltonian. $\gamma=0.01$ in (a)-(c) and 2.2 in (d)-(f). Close to GinUE behaviour observed for $\gamma=2.2$ which is also evident from the marginal distributions, somewhat close to the analytical results plotted with the red dotted line. For $\gamma=0.01$, results are closer to Poisson statistics showing uniform density in the unit circle. The radial distribution also adheres to this result while a slight dip at the origin is noted for the angular distribution plot.

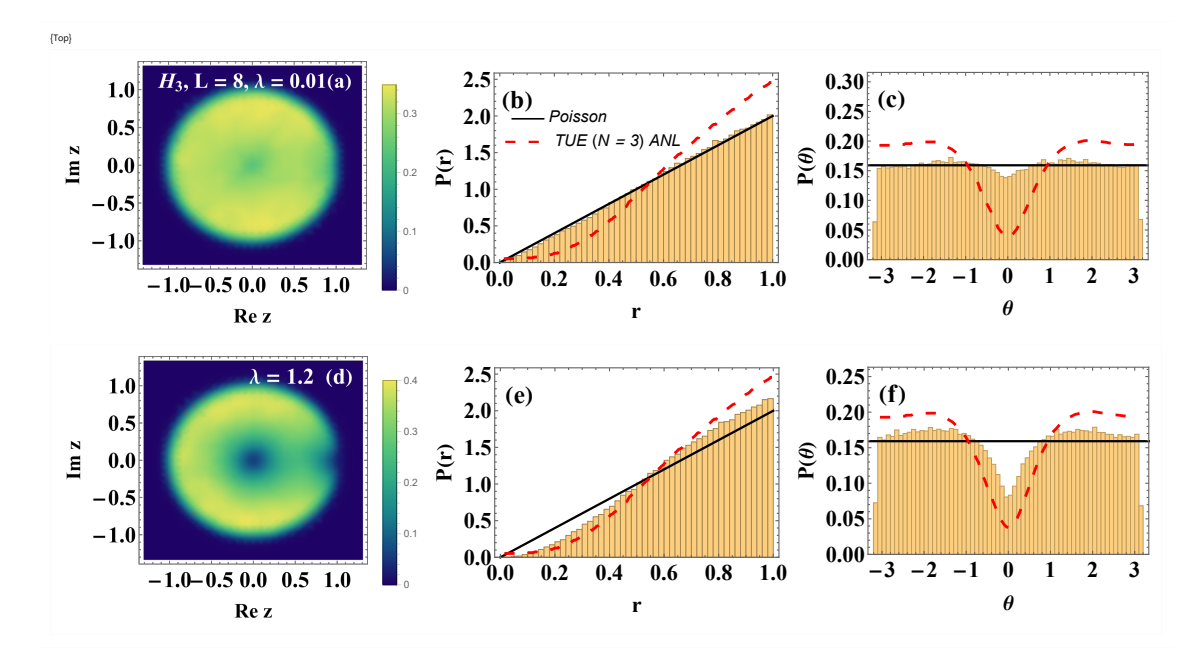


FIG. 15. In this case, only λ is varied. Poisson like behaviour is much more prominent for $\lambda = 0.01$ and GinUE like behaviour is observed for $\lambda = 1.2$ which is also evident from radial and angular marginal distributions.

increasing system dimension. A more thorough exploration is one of our future ventures.

Thirdly, the *n*-dimensional 1D and 2D-Poisson to GinUE interpolating ensembles model the spectral crossovers shown by the spin chains very well. This can be seen by comparing the plots from matrix model sim-

ulations with those from the spin chains. These kind of interpolating models are already known for Poisson-GOE and Poisson-semi-Poisson distributions. The first matrix model interpolating 1D-Poisson to GinUE is particularly interesting in the context of real to complex eigenvalue-kind of transitions which have been discussed

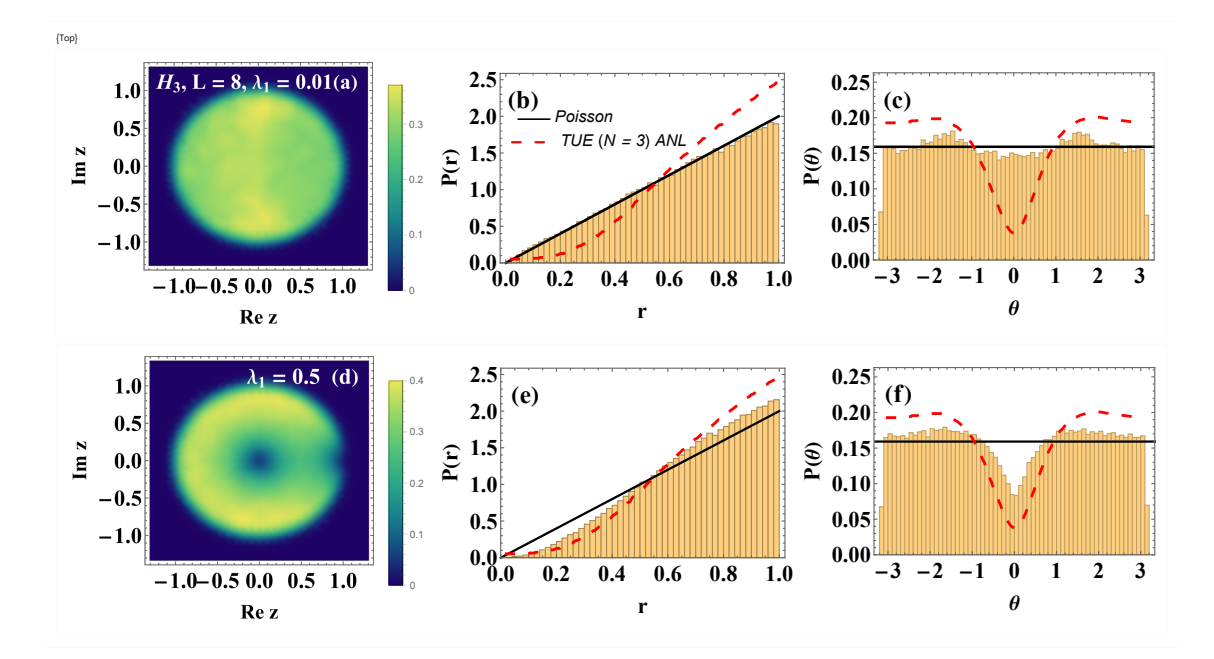


FIG. 16. Here λ_1 is varied and subtle expressions of GinUE-like statistics is noted for $\lambda_1 = 0.5$ in (d)-(f) while Poisson like statistics is observed for $\lambda_1 = 0.01$ and the angular marginal distribution shows deviations, not as evident in CSR density plot.

λ	$\langle r angle$	$-\langle\cos\theta\rangle$
0.001	0.673623	-0.017631
0.9	0.712756	0.040116
3	0.66796	-0.153083
γ	$\langle r angle$	$-\langle\cos\theta\rangle$
0.01	0.563826	0.35562
0.5	0.689789	0.00216
3	0.662463	0.093938
λ_1	$\langle r angle$	$-\langle \cos \theta \rangle$
0.001	0.651133	0.008625
0.1	0.665952	0.008774
4	0.681085	-0.13942

TABLE II. Single number signatures of $H_2, L=6$ for parameter values corresponding to the plots.

in the context of many-body localization transition in non-hermitian systems. This transition has previously been used as a diagnostic tool to understand many-body localization in hard-core boson models [74]. It will be of interest to see whether the same can be used to understand ergodicity and many-body localization in our spin chain models. Another intriguing problem would be to attempt to see whether exact crossover matrix model results can be deduced for Poisson-GinUE statistics.

γ	$\langle r \rangle$	$-\langle\cos\theta\rangle$
0.01	0.559528	0.219957
2.1	0.714393	0.062372
λ	$\langle r angle$	$-\langle\cos\theta\rangle$
0.01	0.674636	0.005777
1.2	0.715582	0.080050
λ_1	$\langle r \rangle$	$-\langle\cos\theta\rangle$
0.001	0.659805	0.019756
0.5	0.704006	0.057092

TABLE III. Single number signatures of the H_2 , L=8, for parameter values corresponding to the plots.

γ	$\langle r angle$	$-\langle\cos\theta\rangle$
0.01	0.68242	0.028252
2.2	0.710423	0.06425
λ	$\langle r \rangle$	$-\langle\cos\theta\rangle$
0.01	0.67465	-0.006932
1.2	0.706687	-0.065590
λ_1	$\langle r \rangle$	$-\langle\cos\theta\rangle$
0.01	0.662038	-0.014622
0.5	0.704867	-0.062390

TABLE IV. Single number signatures of the H_3 , L=8, corresponding to the plots shown previously.

ACKNOWLEDGMENTS

AS acknowledges the research fellowship from DST-INSPIRE (IF170612), Govt of India and expresses grati-

tude to Prof. Manas Kulkarni with whom she had fruitful discussions while participating in the program - Statistical Physics of Complex Systems at ICTS, Bangalore (code: ICTS/SPCS2022/12).

- C.M. Bender and S. Boettcher, Phys. Rev. Lett. 80, 5243 (1998).
- [2] C. M. Bender, S. Boettcher, and P. N. Meisinger, J. Math. Phys. 40, 2201 (1999).
- [3] P. Dorey, C. Dunning, and R. Tateo, J. Phys. A: Math. Gen. 34, L391 (2001); 34, 5679 (2001).
- [4] C. M. Bender, D. C. Brody, and H. F. Jones, Phys. Rev. Lett. 89, 270401 (2002).
- [5] C. M. Bender, D. C. Brody, and H. F. Jones, Am. J. Phys 71(11), 1095 (2003).
- [6] A. Fring, Phil Trans R Soc A 371: 20120046 (2013).
- [7] C. M. Bender, PT symmetry: In quantum and classical physics, World Scientific, London, 2019.
- [8] A. Mostafazadeh, J. Math. Phys. 43, 3944 (2002).
- [9] A. Mostafazadeh, J. Math. Phys. 43, 205 (2002).
- [10] A.Mostafazadeh and A. Batal, J. Phys. A:Math. Gen. 37, 11645 (2004).
- [11] A. Mostafazadeh, J. Phys. A: Math. Gen. 36, 7081 (2003).
- [12] H. F. Jones, J. Phys. A: Math. Gen. 38, 1741 (2005).
- [13] N. Hatano and D. R. Nelson, Phys. Rev. Lett. 77, 570 (1996); Phys. Rev. B 56, 8651 (1997).
- [14] D. R. Nelson and N. M. Shnerb, Phys. Rev. E 58, 1383 (1998).
- [15] T. T. Wu, Phys. Rev. 115, 1390 (1959).
- [16] T. Hollowood, Nucl. Phys. B 384, 523 (1992).
- [17] M. E. Fisher, Phys. Rev. Lett. 40, 1610 (1978).
- [18] J. L. Cardy, Phys. Rev. Lett. 54, 1345 (1985).
- [19] J. L. Cardy and G. Mussardo, Phys. Lett. B225, 275 (1989).
- [20] A. B. Zamolodchikov, Nucl. Phys. B **348**, 619 (1991).
- [21] R. Brower, M. Furman, and M. Moshe, Phys. Lett. B76, 213 (1978).
- [22] B. Harms, S. Jones, and C.-I. Tan, Nucl. Phys. 171, 392 (1980); Phys. Lett. B 91, 291 (1980).
- [23] U. Guenther, F. Stefani, and M. Znojil, J. Math. Phys. 46, 063504 (2005).
- [24] U. Guenther, B. F. Samsonov, and F. Stefani, J. Phys. A: Math. Theor. 40, F169 (2007).
- [25] C. F. M. Faria and A. Fring, Laser Physics 17, 424 (2007).
- [26] O. A. Castro-Alvaredo and A. Fring, J.Phys.A 42, 465211 (2009).
- [27] G. von Gehlen, J. Phys. A 24, 5371 (1991).
- [28] G. von Gehlen, Int. J. Mod. Phys. B 8, 3507 (1994).
- [29] C. F. Pai, L. Liu, Y. Li, H. W. Tseng, D. C. Ralph, and R. A. Buhrman, Appl. Phys. Lett. 101, 122404 (2012).
- [30] L. Liu, C. F. Pai, Y. Li, H. W. Tseng, D. C. Ralph, and R. A. Buhrman, Science 336, 555 (2012).
- [31] B. Buca, C. Booker, M. Medenjak and D. Jaksch, New. J. Phys. 22, 123040 (2020).
- [32] M. Nakagawa, N. Kawakami, and M. Ueda, Phys. Rev. Lett. 126, 110404 (2021).
- [33] G. L. Giorgi, Phys. Rev. B 82, 052404 (2010).

- [34] X. Z. Zhang, L. Jin, and Z. Song, Phys. Rev. A 85, 012106 (2012).
- [35] M. Christandl, N. Datta, A. Ekert, and A. J. Landahl, Phys. Rev. Lett. 92, 187902 (2004).
- [36] M. Christandl, N. Datta, T. C. Dorlas, A. Ekert, A. Kay, and A. J. Landahl, Phys. Rev. A 71, 032312 (2005).
- [37] O. Bendix, R. Fleischmann, T. Kottos, and B. Shapiro, Phys. Rev. Lett. 103, 030402 (2009).
- [38] Y. N. Joglekar, D. Scott, M. Babbey, and A. Saxena, Phys. Rev. A 82, 030103(R) (2010).
- [39] L. Jin and Z. Song, Phys. Rev. A 80, 052107 (2009); 81, 032109 (2010); 84, 042116 (2011); 85, 012111 (2012).
- [40] M. Znojil, J. Phys. A:Math. Theor. 40, 13131 (2007); 41, 292002 (2008); Phys. Rev. A 82, 052113 (2010); J. Phys. A: Math. Theor. 44, 075302 (2011).
- [41] S. Longhi, Phys. Rev. B 80, 235102 (2009); 81, 195118 (2010); Phys. Rev. A 82, 032111 (2010); Phys. Rev. B 82, 041106(R) (2010).
- [42] Y. N. Joglekar and A. Saxena, Phys. Rev. A 83, 050101(R) (2011); D. D. Scott and Y. N. Joglekar, ibid. 83, 050102(R) (2011).
- [43] C. Korff and R. Weston, J. Phys. A: Math. Theor. 40, 8845 (2007).
- [44] H. Zhong, W. Hai, G. Lu, and Z. Li, Phys. Rev. A 84, 013410 (2011).
- [45] L. B. Drissi, E. H. Saidi, and M. Bousmina, J. Math. Phys. 52, 022306 (2011).
- [46] Ö. Yesiltas, J. Phys. A: Math. Theor. 44, 305305 (2011).
- [47] F. Bagarello and M. Znojil, J. Phys. A: Math. Theor. 44, 415305 (2011).
- [48] W. H. Hu, L. Jin, Y. Li, and Z. Song, Phys. Rev. A 86, 042110 (2012).
- [49] X. Z. Zhang and Z. Song, Phys. Rev. B 87, 012114 (2013).
- [50] X. Z. Zhang and Z. Song, Phys. Rev. A 88, 042108 (2013).
- [51] E. Lange, G. Chimczak, A. Kowalewska-Kudłaszyk and K. Bartkiewicz, Sci. Rep. 10, 19906 (2020).
- [52] X. Peng, H. Zhou, B.-B. Wei, J. Cui, J. Du, and R.-B. Liu, Phys. Rev. Lett. 114, 010601 (2015).
- [53] A. Galda and V. M. Vinokur, Phys. Rev. B 97, 201411(R) (2018).
- [54] D. A. Rabson, B. N. Narozhny, and A. J. Millis, Phys. Rev. B 69, 054403 (2004).
- [55] R. Modak and S. Mukherjee, New J. Phys. 16, 093016 (2014).
- [56] Y. Avishai, J. Richert, and R. Berkovits, Phys. Rev. B 66, 052416 (2002).
- [57] K. Kudo and T. Deguchi, Phys. Rev. B 69, 132404 (2004).
- [58] M. Serbyn and J. E. Moore, Phys. Rev. B 93, 041424(R) (2016).
- [59] R. Modak, S. Mukerjee, and S. Ramaswamy, Phys. Rev. B 90, 075152 (2014).
- [60] N. Regnault and R. Nandkishore, Phys. Rev. B 93, 104203 (2016).

- [61] D. J. Luitz, N. Laflorencie, and F. Alet, Phys. Rev. B 91, 081103(R) (2015).
- [62] M. Žnidarič, T. Prosen, and P. Prelovšek, Phys. Rev. B 77, 064426 (2008).
- [63] M. L. Mehta, Random Matrices, 3rd ed. (Elsevier, Amsterdam, 2004).
- [64] L. Sá, P. Ribeiro and T. Prosen, Phys. Rev. X. 10, 021019 (2020).
- [65] V. Oganesyan and D. A. Huse, Phys. Rev. B 75, 155111 (2007).
- [66] Y. Y. Atas, E. Bogomolny, O. Giraud, G. Roux, Phys. Rev. Lett. 110, 084101 (2013).
- [67] Y. Y. Atas, E. Bogomolny, O. Giraud, P. Vivo and E. Vivo, J. Phys. A: Math. Theor. 46 355204 (2013).
- [68] A. Sarkar, M. Kothiyal, and S. Kumar, Phys. Rev. E 101, 012216 (2020).
- [69] S. C. L. Srivastava, A. Lakshminarayan, S. Tomsovic, and A. Bäcker, J. Phys. A 52, 025101 (2018).
- [70] A. M. García-García, L. Sá and J. J. M. Verbaarschot, Phys. Rev. X. 12 (2), 021040 (2022).

- [71] L. Sá and A. M. García-García, Phys. Rev. D. 105 (2), 026005 (2022).
- [72] I. G. Dusa and T. Wettig, Phys. Rev. E 105, 044144 (2022).
- [73] R. Hamazaki, K. Kawabata, N. Kura, and M. Ueda, Phys. Rev. Res. 2, 023286 (2020).
- [74] R. Hamazaki, K. Kawabata, M. Ueda, Phys. Rev. Lett. 123, 090603 (2019).
- [75] N. D. Chavda and V. K. B. Kota, Phys. Lett. A. 377 3009 (2013).
- [76] N. D. Chavda, H. N. Deota, V. K. B. Kota, Phys. Lett. A, 378 41 (2014)
- [77] K. Roy et. al. EPL 118 46003 (2017).
- [78] Y. V. Fyodorov, B. A. Khoruzhenko, and H.-J. Sommers, Phys. Rev. Lett. 79, 557 (1997).
- [79] S.-S. Byun and M. Ebke, arXiv preprint, arXiv 2108.05541 (2021).
- [80] G. Akemann, M. Duits, L. D. Molag, arXiv preprint, arXiv:2203.00287 (2022).
- [81] S.-S. Byun and P. J. Forrester, arXiv preprint, arXiv 2211.16223 (2022).